Multigroup Energy Representation for Fast Monte Carlo Estimation of Radioisotope Yields From Electron-Beam Spectra

Bruno Silveira Nunes, Nilson Dias Vieira Junior, Alexandre Bonatto, and Ricardo Elgul Samad

***Abstract*—Monte Carlo (MC) simulations are widely used to estimate radioisotope production through nuclear reactions. However, achieving high accuracy typically requires simulating more than 10^8 particles, which is computationally demanding, particularly when many simulations are required, such as in optimization loops. In a previous study, we demonstrated that molybdenum-99 yields from bremsstrahlung-driven photonuclear reactions induced by laser accelerated electron beams can be estimated up to four orders of magnitude faster by employing a multigroup energy representation, in which a limited set of MC precomputed group yields is used to reconstruct the total yield for an arbitrary source spectrum. This work expands this approach by showing that the multigroup representation also provides a deeper understanding of the relative contribution of different electron energies to the final isotope yield. Applying the method to 640 different spectra revealed how the choice of group structure—such as the number of groups and their energy widths—affects both accuracy and efficiency. The results show that the proposed approach reproduces full MC yield estimates with median errors below 5%, reaching values as low as 0.3%.**

***Index Terms*—Laser wakefield acceleration (LWFA), molybdenum-99, Monte Carlo (MC) simulation, multigroup energy, radioisotope production.**

I. Introduction

CURRENTLY, the global supply chain of radioisotopes for nuclear medicine relies heavily on nuclear research reactors [1], which generate radionuclides from the uranium-235 (^{235}U) fission [2]. Particularly, ~6% of the ^{235}U fission products are molybdenum-99 atoms (^{99}Mo, half-life of 66 h), which decay into technetium-99m (^{99m}Tc, metastable, half-life of 6 h). ^{99m}Tc is the most widely used radioisotope in nuclear medicine, with over 40 million single-photon emission computed tomography (SPECT) [3] procedures annually. The relatively long half-life of ^{99}Mo facilitates worldwide distribution via ^{99}Mo/^{99m}Tc generators [4], implying in a centralized production. However, ^{99}Mo production depends on highly enriched uranium (HEU), and many of the reactors responsible for its supply were built in the 1970s and are at the end of their useful lives, demanding constant maintenance and raising concerns about aging infrastructure [5].

In 2009, the simultaneous shutdown of the two largest research reactors caused a global shortage of ^{99}Mo, highlighting the fragility of the radioisotope supply chain [6]. To address this vulnerability, alternative production methods, especially those that avoid the use of HEU [7], have been under development. One promising strategy to decentralize production and reduce reliance on research reactors involves using accelerated electrons to induce nuclear reactions that produce ^{99}Mo from the naturally-occurring, stable isotope ^{100}Mo [8]. When electrons with energy of tens of megaelectronvolts hit a converter made of a large atomic number material such as tantalum ($Z = 73$), bremsstrahlung-generated gamma rays can induce the ^{100}Mo(γ, n)^{99}Mo photonuclear reaction on an Mo target [9], [10], [11], [12].

A promising approach to accelerate electrons is the use of laser wakefield acceleration (LWFA) [13], [14] driven by few-terawatt, high-repetition-rate ultrashort laser pulses. In this process, a laser pulse is focused in a gas jet in a vacuum environment, creating a plasma capable of sustaining longitudinal electric fields that can reach TV/m [14], [15] and accelerate electrons to high energies over short distances. By impinging these high-energy electrons on a converter, bremsstrahlung photons are produced that can, depending on their energies, trigger photonuclear reactions that convert ^{100}Mo atoms into ^{99}Mo. This process involves complex interdependencies among multiple parameters, such as laser pulse intensity and focusing, gas target density and dimensions, and converter and target geometry. Given that experimental optimization is both laborious and time-intensive, this physical system is particularly suitable for numerical simulation approaches.

An effective strategy for investigating how variations in initial laser and plasma conditions affect the electron beam—and, consequently, bremsstrahlung and radioisotope production—is to combine particle-in-cell (PIC) [16] and Monte Carlo (MC) simulations [17]. PIC simulations solve the equations of motion for charged particles under the Lorentz force, using self-consistent electromagnetic fields computed on a spatial grid by discretizing and solving Maxwell's equations. This approach enables accurate modeling of laser-driven electron

Received 13 March 2026; accepted 17 March 2026. Date of publication 20 March 2026; date of current version 24 April 2026. This work was supported in part by the Conselho Nacional de Desenvolvimento Científico e Tecnológico (CNPq) under Grant 405143/2021-4 and Grant 140941/2023-1 and in part by the Fundação de Amparo à Pesquisa do Estado do Rio Grande do Sul (FAPERGS) under Grant 24/2551-0001552-3. *(Corresponding author: Bruno Silveira Nunes.)*

Bruno Silveira Nunes, Nilson Dias Vieira Junior, and Ricardo Elgul Samad are with the Nuclear and Energy Research Institute, IPEN–CNEN, São Paulo 05508-000, Brazil (e-mail: brunosnunes@usp.br; rsamad@usp.br).

Alexandre Bonatto is with the Federal University of Health Sciences of Porto Alegre (UFCSPA), Porto Alegre 90050-170, Brazil.

Color versions of one or more figures in this article are available at https://doi.org/10.1109/TNS.2026.3675947.

Digital Object Identifier 10.1109/TNS.2026.3675947

acceleration, providing as output, for example, the energy spectra of LWFA-accelerated beams. These spectra can then be used as radiation sources in MC simulations, which model the interaction of particle and radiation beams with matter using a probabilistic approach to trace potential outcomes in the history of a particle or a photon. By evaluating reaction cross sections, MC simulations estimate the number of bremsstrahlung photons and radioisotopes, such as ^{99}Mo, produced by nuclear reactions [18]. Since finding optimal conditions for ^{99}Mo production with the proposed combined-simulation framework requires exploring a large parameter space and each simulation is computationally expensive, an effective strategy to reduce this cost is to integrate the framework with Bayesian optimization.

Optimization algorithms, particularly Bayesian ones, efficiently navigate the vast parameter spaces characteristic of the physical systems under study by iteratively sampling and converging on promising regions [19]. By stating the problem as the maximization of an objective function that rewards desirable outcomes and penalizes undesirable ones, these algorithms can identify optimal parameters through iterative simulation-optimization cycles.

In a previous work [20], Bayesian optimization was applied to iterative PIC simulations to maximize the energy and charge of LWFA-accelerated electron beams. After identifying optimal beam parameters, the resulting electron spectra were used to compute the bremsstrahlung photon production in a tantalum converter and subsequently calculate the yield of ^{99}Mo through the ^{100}Mo $(\gamma, n)^{99}$Mo nuclear reaction induced by these photons. While adding the MC simulations to the optimization loop would allow for the direct use of the ^{99}Mo yield as the objective function to be maximized, this strategy would significantly increase the computational cost. Depending on the available hardware, simulation domain, and so on, even GPU-accelerated PIC codes can require hours to days of runtime, and CPU-bound MC simulations—often tracking 10^8 particles for statistical accuracy—also take many hours per run. As a result, each optimization iteration is costly, and the full simulation-optimization cycle can demand a long computation time.

To address the computational time challenges in MC simulations, a previous study from our group [21] demonstrated that a multigroup energy representation can be used to estimate MC results of radioisotope production from electron beam energy spectra in a fraction of a second, providing results equivalent to those obtained with a large number of particles. This work expands the previous study discussing the size of the multigroup, presents a deeper error analysis, and shows that this approach highlights the contribution of each electron energy to the final isotope production.

II. Simulations and Methodology

In this study, 640 electron energy spectra with varying shapes, charges, and maximum energies were obtained from PIC simulations using the Fourier-Bessel PIC (FBPIC) code [22]. The simulations explored different initial conditions for the gas jet and laser focal position. Each employed a 10 TW peak-power Gaussian laser pulse with a full-width at half-maximum (FWHM) intensity duration of 35 fs, with a wavelength of 800 nm, linearly polarized along the x-axis and propagating along the z-axis, focused to a 7 μm beam waist. The laser propagates through a gas jet with a trapezoidal density profile [23], composed of a helium-nitrogen mixture with varying total and relative densities (relative mass ratios from 0% to 100%) [24], and different lengths. These parameters were chosen in accordance with the design of a laser-plasma accelerator currently under development at the Center for Lasers and Applications of the Nuclear and Energy Research Institute (IPEN-CNEN, Brazil).

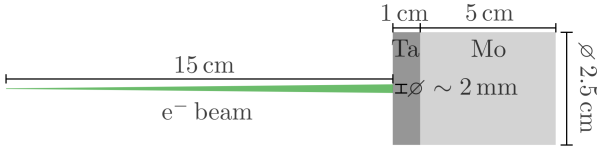

Fig. 1. Beam-target configuration (not to scale).

The electron energy spectra were used as inputs for MC simulations in openTOPAS v4.0.0 (Tool for Particle Simulation) [25], [26], a Geant4-based toolkit [27]. In these simulations, electrons were generated from a particle source defined with a Gaussian spatial distribution, specific divergences, and particle energies determined by the FBPIC generated spectra. The source produces cylindrical electron beams with a Gaussian radial distribution $f(r) = e^{-r^2/2\sigma^2}$, where $\sigma = 30$ μm is the standard deviation. The beam radius is defined as 2σ, encompassing approximately 86% of the electrons, and has 3.2 mrad of angular divergence in both the x- and y-directions. The beam propagates through 15 cm of vacuum before reaching a cylindrical tantalum (Ta) converter with a radius of 1.25 cm and a thickness of 1 cm, as illustrated in Fig. 1. At the point of impact, the beam has a diameter of 1.92 mm (corresponding to 4σ of the transverse distribution), consistent with typical LWFA beam characteristics. Immediately after the converter, a cylindrical natural molybdenum (^{nat}Mo, which contains 9.7% of ^{100}Mo) target with identical transverse dimensions and a thickness of 5 cm is positioned. Although ^{100}Mo-enriched is available, its cost is significantly higher than that of natural molybdenum. Considering the 9.7% abundance of ^{100}Mo in ^{nat}Mo, the yield from a fully enriched target may be approximated by scaling the ^{nat}Mo results by one order of magnitude. The radii of the Ta and ^{nat}Mo targets were chosen to balance realistic dimensions with minimal electron losses from large-angle scattering. The converter thickness was chosen to enable the analyses of production and absorption of photons for different electron beams, while the ^{nat}Mo target thickness was designed to maximize the ^{99}Mo yield.

Let $\psi(\mathcal{E})$ represent one of the 640 input spectra, used as the radiation source in an MC simulation to estimate the ^{99}Mo yield, Y_{spec}. By choice, $\psi(\mathcal{E})$ begins at 8 MeV since electrons below this threshold cannot produce bremsstrahlung photons energetic enough to trigger the ^{100}Mo$(\gamma, n)^{99}$Mo reaction. The cross section of this reaction becomes significant between 8 and 20 MeV, reaching its maximum at 14.5 MeV [9].

Although each input spectrum carries a total charge (Q_{tot}) on the order of nC, i.e., about 10^{10} electrons, it can be efficiently modeled in an MC simulation using $N_e = 10^8$ histories, each representing the evolution of one electron, with a weight factor W_{MC} to scale the simulation results accordingly

$$W_{\text{MC}} = \frac{Q_{tot}}{eN_e} \tag{1}$$

where e is the elementary charge. In this way, every MC result is multiplied by W_{MC} to obtain an estimate of the result for the correct number of particles.

A good approximation of Y_{spec}, the ^{99}Mo yield obtained from the MC simulation of an electron beam with an energy spectrum $\psi(\mathcal{E})$ can be achieved using a multigroup energy discretization method. In the approach presented here, the energy domain is divided into discrete groups of constant width $\Delta\mathcal{E}$, and each group is independently propagated through the same physical system by an MC simulation. This procedure returns a corresponding ^{99}Mo production yield y_i for the ith energy group. The total multigroup yield is then computed as

$$Y_g = \sum_i a_i y_i, \quad i = 0, 1, 2, \ldots \tag{2}$$

where a_i corresponds to the number of particles contained in the ith energy group, obtained by integrating the spectral distribution over the group interval [28], [29]

$$a_i = \int_{i\Delta\mathcal{E}}^{(i+1)\Delta\mathcal{E}} \psi(\mathcal{E})\, d\mathcal{E}. \tag{3}$$

Further details on the multigroup discretization and its physical interpretation are provided in the Appendix for readers not familiar with this formalism.

For a given multigroup, the accuracy of Y_g can be evaluated by comparing it with the reference Y_{spec}. The relative error between these two yields, ϵ, is calculated by

$$\epsilon\ [\%] = 100\frac{Y_g - Y_{\text{spec}}}{Y_{\text{spec}}}. \tag{4}$$

A negative error value indicates that the multigroup underestimates the ^{99}Mo production, while a positive error denotes an overestimation.

To assess the accuracy and limitations of the multigroup energy representation method, five energies groups with different resolutions, $\Delta\mathcal{E} = \{0.25, 0.5, 1, 2, 5\}$ MeV, were precomputed through MC simulations, providing the corresponding y_i values [in (2)]. The 640 spectra were then discretized onto each multigroup, and the results were analyzed as a function of $\Delta\mathcal{E}$. The discretizations and yield estimates Y_g [in (2)] were carried out using a Wolfram Mathematica 14.0 script.

While the multigroup with $\Delta\mathcal{E} = 5$ MeV spans the energy interval from 8 to 258 MeV, the remaining multigroups extend from 8 to 260 MeV, covering the energy range of all projected spectra.

For each element of every multigroup, an MC simulation was performed with $p = 10^6$ particles uniformly distributed over its energy width ($i\Delta\mathcal{E} \leq \mathcal{E} < (i+1)\Delta\mathcal{E}$). For a multigroup with k elements, the total number of simulated particles per group amounts to $k \cdot p \approx 10^7 - 10^9$ particles, depending on

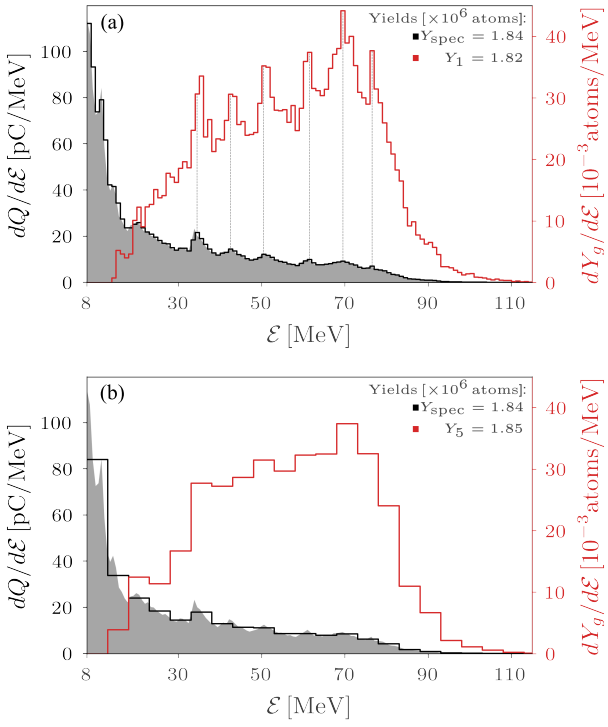

Fig. 2. Discretization of an electron spectrum (gray shaded area) onto (a) 1 MeV multigroup and (b) 5 MeV multigroup, with the corresponding discretizations shown as a black line. The resulting ^{99}Mo yields for each group are depicted in red.

$\Delta\mathcal{E}$. The cost of precomputing all elements of a multigroup is comparable to that of performing a few conventional MC simulations with 10^8 histories. However, since the optimization process may require hundreds of iterations [20], the use of a precomputed multigroup can substantially reduce the computational time needed to reach the optimal solution.

III. Results and Discussion

Fig. 2 shows a representative spectrum of the 640 obtained from the PIC simulations (gray shaded area) and the results of discretizing it onto the multigroups with $\Delta\mathcal{E}$ of (a) 1 MeV and (b) 5 MeV. In both figures, the black line represents the spectrum discretization onto the multigroup, while the red line shows the corresponding yield for each group, $a_i y_i$. The total yields from the spectrum (Y_{spec}) and those estimated from the multigroup (Y_g, with g being the group width $\Delta\mathcal{E}$) are also shown. The values estimated from the multigroups differ from the reference yield Y_{spec} by -1.1% and 0.5% for the 1 and 5 MeV multigroups, respectively. While running an MC simulation with the original spectrum yields the reference ^{99}Mo production, Y_{spec}, the discretization of the spectrum onto a precomputed multigroup provides a deeper understanding. In this approach, a yield is obtained for each group, and the resulting set of yields can be interpreted as a yield function—or the multigroup representation of the energy-dependent importance function for the production of ^{99}Mo nuclei from source beam electrons [30] (red curves in Fig. 2)—which highlights which energies contribute most to the ^{99}Mo production. This decomposition reveals a threshold

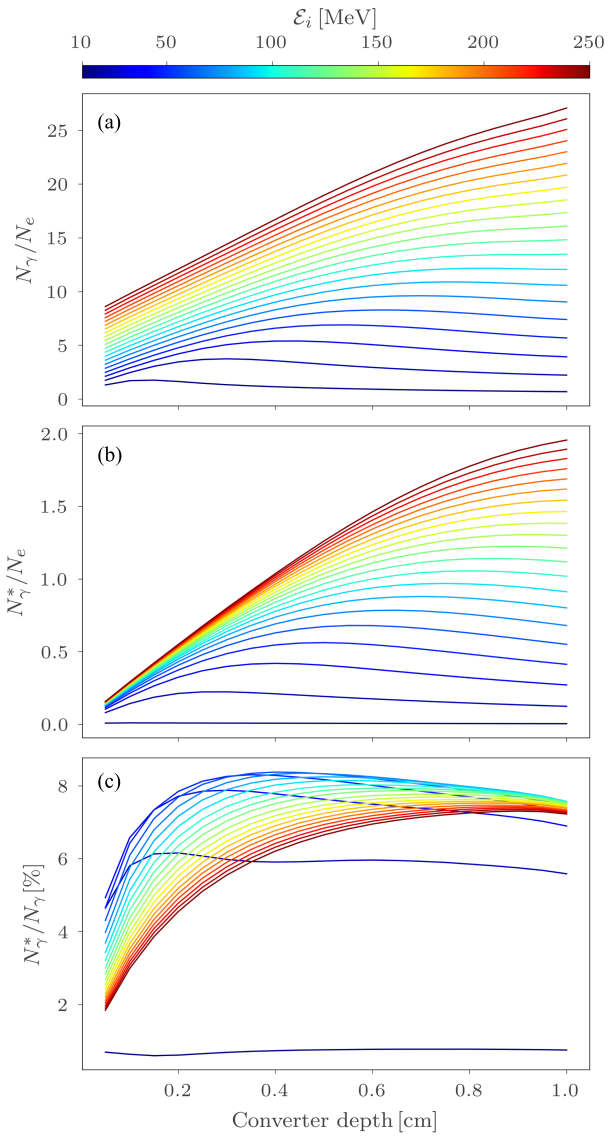

Fig. 3. Cumulative photon production along the tantalum converter, normalized by the number of electrons of the multigroup element (a) all photons, (b) photons with energies between 8 and 20 MeV (resonant with the ^{100}Mo$(\gamma, n)^{99}$Mo reaction), and (c) fraction of photons within this resonant range. Each line represents the simulation of a 1 MeV multigroup element using 10^6 electrons, with the color scale indicating their initial energy.

at approximately 13 MeV, below which electrons do not have sufficient energy to produce bremsstrahlung photons capable of triggering ^{99}Mo production. Above 20 MeV, the yield function exhibits a strong correspondence with the electron spectrum: all spectral peaks, including minor ones, give rise to counterpart peaks in the yield function, as indicated by the vertical dashed lines in Fig. 2(a). In Fig. 2(b), the broader multigroup reduces the energy resolution, making the correspondence less distinct but still evident. The results in Fig. 2 also demonstrate that higher-energy electrons are more efficient at producing ^{99}Mo: despite their smaller charge compared to lower-energy peaks, their contribution to the total yield is greater. This trend extends up to $\sim$ 80 MeV, beyond which the efficiency of ^{99}Mo generation decreases due to the declining number of electrons at higher energies.

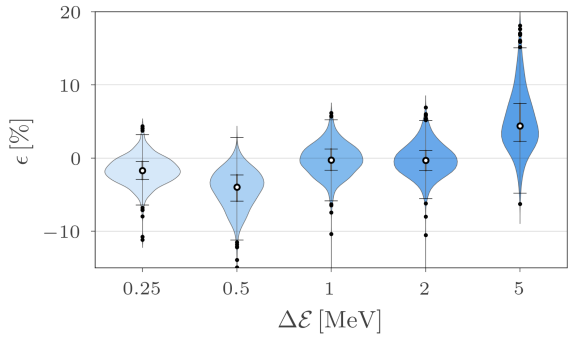

Fig. 4. Violin plots of the errors in yield estimation: comparison between the spectral yield and the estimated yields of the five multigroups' discretization.

Fig. 3 shows the number of bremsstrahlung gamma photons, N_γ, as a function of the tantalum converter depth, taking into account their production and absorption. Each curve corresponds to an element of the $\Delta\mathcal{E}$ = 1 MeV multigroup. This subset spans the full energy range and was chosen to avoid clutter. The curves were obtained using 20 phase-space detectors positioned along the converter thickness from 0.05 to 1 cm. In Fig. 3(a), each curve represents the total number of gamma photons at a given depth, normalized by the initial number of electrons N_e in the corresponding group (with initial energy $\mathcal{E}_i$, indicated by the color scale). Fig. 3(b) shows the number of photons generated per incident electron in the 8–20 MeV, N^*_γ/N_e, which corresponds to the resonance range of the ^{100}Mo$(\gamma, n)^{99}$Mo reaction [9], [12]. These graphs show that as the electron energy increases, both the total photon yield and the photon yield in the resonance interval grow. This yield boost occurs because the electron bremsstrahlung cross section has a complex dependence on the electron energy, rising with it [31], which, in turn, increases the total number of photons produced. Furthermore, bremsstrahlung photons can interact with the converter atoms, generating secondary electrons by the photoelectric absorption, Compton scattering, and pair production, with each process probability depending on the photon energy [32]. These secondary electrons generate additional bremsstrahlung photons. Consequently, the probability of producing a 14 MeV photon (the ^{100}Mo$(\gamma, n)^{99}$Mo cross section peak) through multiple interactions of a high-energy electron is significantly higher than the probability of a single 14 MeV electron producing an equivalent photon by a direct collision—an extremely rare process. Fig. 3(b) illustrates this by revealing that while two electrons with energy of approximately 75 MeV are needed to produce one resonant photon (8–20 MeV) at the converter exit (1 cm depth), a single 250 MeV electron generates two resonant photons at this position. In addition, the electron penetration depth in the converter rises with its energy, and therefore, the converter's optimal thickness depends on the energy of the incident electrons, balancing increased photon production with absorption losses inside it. Finally, Fig. 3(c) displays the ratio of photon counts in (a) and (b), N^*_γ/N_γ. For initial electron energies above 70 MeV, this fraction converges to about 7.5% with little dependence on energy, while it decreases sharply at lower energies.

Fig. 4 shows the distributions of relative errors between the multigroup-estimated ^{99}Mo yields (Y_g), obtained using the five different multigroups, and the reference yields from standard MC simulations (Y_{spec}), as defined in (4). Each distribution, constructed from the relative errors of the 640 input electron spectra, is presented as a violin plot. The central hollow dot indicates the median, horizontal lines represent the first and third quartiles and distribution bounds, and outliers appear as black dots. Looking at the violin plot, the accuracy of multigroup-estimated ^{99}Mo yields shows a complex dependence on the multigroup width ($\Delta\mathcal{E}$). For $\Delta\mathcal{E}$ = 0.25 MeV, the distribution exhibits a negative bias with a median error around −1% and a small spread, with outliers extending to approximately −10%. For $\Delta\mathcal{E}$ = 0.5 MeV, the distribution becomes more asymmetric and is centered farther from zero, showing a slight negative bias around −3%. The distributions for $\Delta\mathcal{E}$ = 1 and 2 MeV show improved centering with medians near 0%, similar narrow spreads, with errors ranging from −6.0% to 5.3% and fewer outliers, suggesting better overall accuracy at these intermediate resolutions. However, at the coarsest resolution ($\Delta\mathcal{E}$ = 5 MeV), the accuracy and dispersion deteriorate significantly. The median error increases to almost 5%, representing the largest systematic bias among all tested multigroups. In addition, this configuration shows increased positive outliers extending beyond 15%, and the overall distribution width is approximately double that of the other multigroups. This degradation at the coarsest multigroup width suggests that while the multigroup energy discretization method shows robustness across a range of energy resolutions, excessive coarsening of the resolution leads to loss of important spectral information needed for accurate yield estimation. Nevertheless, even with this smaller accuracy, the error between the first and third quartiles is under 10%, providing good estimates of the ^{99}Mo yield.

The optimal results occur at intermediate bin widths (1–2 MeV), where the balance between spectral resolution and statistical stability produces the most accurate and consistent yield estimates with minimal systematic bias and reduced scattering.

The main advantage of using multigroup energy discretization to estimate spectral yields is the substantial time savings in repetitive or recursive calculations, such as solving optimization problems iteratively. The average runtime of a full MC simulation for the set of 640 spectra—each of them executed with 10^8 electrons, on 24 threads of an AMD Ryzen 9 12-core processor (@ 4.8 GHz) with 64 GB RAM—was 33 min. In contrast, once the multigroup energy representation had been precomputed, and the corresponding y_i yields obtained, discretizing a spectrum onto the multigroup and estimating its yield required only 0.65, 0.38, 0.23, 0.16, and 0.12 s for $\Delta\mathcal{E}$ = 0.25, 0.5, 1, 2, and 5 MeV, respectively, when executed via a Mathematica script on the same machine. The execution time scaled approximately with $\Delta\mathcal{E}^{-1}$, corresponding to speedups of ∼ 3000×, 5200×, 8600×, 12 400×, and 16 500× compared with a full openTOPAS simulation.

The average time to compute a single group with 10^6 electrons on the same machine is about 2 min, regardless of the multigroup size. Hence, the payback time for precomputing the multigroup depends on the number of elements in it. For an energy range of ∼ 250 MeV (which covers all the input spectra), the computational cost is recovered after running 61, 31, 15, 8, and 3 full-spectrum MC simulations—each with 10^8 electrons—for the multigroups with $\Delta\mathcal{E}$ = 0.25, 0.5, 1, 2, and 5 MeV, respectively, a relatively small number of simulations in the context of optimization problems.

Taking into account the errors shown in Fig. 4 and the time needed to simulate the multigroup, the 2 MeV multigroup optimizes the solution for the problem presented here, considering both the projection of the spectra and the time payback.

Each group is simulated with 10^6 electrons. Thus, covering the 250 MeV energy range with $\Delta\mathcal{E}$ = 2 MeV requires about 125 simulations, corresponding to a total of ∼ 10^8 particles. This matches the number of particles used to compute the reference yield Y_{spec}, which explains the good agreement obtained for $\Delta\mathcal{E}$ = 1 and 2 MeV. In contrast, using $\Delta\mathcal{E}$ = 0.25 MeV would require roughly 1000 simulations or ∼ 10^9 particles—an order of magnitude larger than that used for Y_{spec}. This imbalance likely accounts for the larger discrepancies observed in this case. A similar issue arises for $\Delta\mathcal{E}$ = 5 MeV, which requires only about 50 simulations, corresponding to ∼ 5×10^7 particles, i.e., half of those used for Y_{spec}. This factor of two reduction applies if the spectrum spans the full 250 MeV range. For spectra with lower maximum energies, the discrepancy is even greater: for instance, with a 100 MeV cutoff, the cumulative number of simulated particles drops to about one quarter of that used for Y_{spec}. Such reductions likely explain the larger errors observed with the widest multigroup.

As a final note, it is common to post-process the results of PIC simulations to obtain a histogram $h(\mathcal{E})$ representing the particle energy distribution, rather than a continuous function $\psi(\mathcal{E})$. Assuming that this histogram has bins with width $\delta\mathcal{E}$ and $h(\mathcal{E}_i)$ is the number of particles—electrons—in the ith bin, when discretizing the spectrum, $\psi(\mathcal{E})$ must be replaced in (3) by the normalized histogram, $h(\mathcal{E})/\delta\mathcal{E}$, which corresponds to the histogram's probability density function (pdf) multiplied by the total number of particles, N_e. This adjustment ensures that any spectrum can be discretized onto the multigroup by substituting $\psi(\mathcal{E})$ by $h(\mathcal{E})/\delta\mathcal{E}$ in (3).

IV. Conclusion

A precomputed multigroup energy discretization can be applied to drastically reduce the computational time required for estimating radioisotope production from an electron energy spectrum through MC simulations. Five different multigroups' energy representations were tested, all achieving accurate production estimates for hundreds of spectra, taking less than a second for each spectrum, representing a speed-up ranging from 3000× to 16 500×, depending on the multigroup size, compared to a full openTOPAS simulation of a single spectrum employing 10^8 histories. This acceleration is particularly suitable for applications requiring rapid yield evaluation or extensive parameter space exploration, such as in optimization scenarios, significantly enhancing the efficiency of iterative processes.

Based on the comparative analysis of 640 electron spectra, the multigroup energy discretization method can rapidly

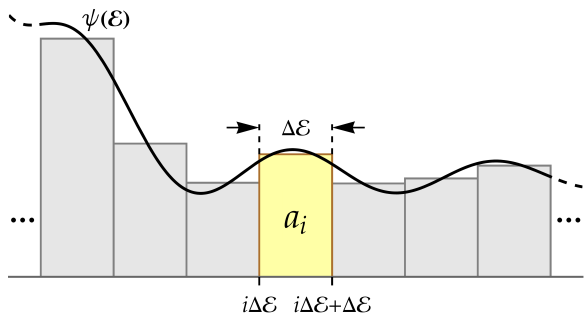

Fig. 5. Illustration of the multigroup discretization of a continuous spectral distribution $\psi(\mathcal{E})$ into energy groups of width $\Delta\mathcal{E}$. The area a_i represents the number of particles contained in the ith energy group, which is also the area of the $\psi(\mathcal{E})$ integral in the group interval. Adapted from [21].

provide accurate estimates of ^{99}Mo production yields, with median relative errors of −1.7%, −4.0%, −0.3%, −0.3%, and 4.4% for multigroups with $\Delta\mathcal{E} = 0.25, 0.5, 1, 2,$ and 5 MeV, respectively. The smallest estimate errors occur for multigroups in which the total number of electrons (number of groups times the number of electrons per group) is close to the number of electrons in an MC simulation of a full spectrum, indicating the multigroup width $\Delta\mathcal{E}$.

This methodology is limited to a fixed physical system; for instance, modifying dimensions such as the converter or Mo thickness requires new simulations of the multigroup. Nonetheless, it is broadly applicable to any physical system that can be modeled with MC simulations and is particularly useful when a large number of simulations are demanded.

Appendix
Derivation and Physical Interpretation of the Multigroup Formulation

Since nuclear reaction rates are proportional to the incident particle flux [28], the ^{99}Mo yield produced by an electron beam with spectral distribution $\psi(\mathcal{E})$ can be obtained by integrating the contribution from each energy component of the spectrum

$$Y_{\text{spec}} = \int_0^{\infty} \psi(\mathcal{E})\, y(\mathcal{E})\, d\mathcal{E} \tag{5}$$

where $y(\mathcal{E})$ denotes the yield produced per particle by an electron with energy $\mathcal{E}$.

In the multigroup representation, the energy domain is partitioned into intervals (groups) of width $\Delta\mathcal{E}$. Within each group, the yield is approximated by a constant value $y_i \approx y(i\Delta\mathcal{E} + \Delta\mathcal{E}/2)$ for $i\Delta\mathcal{E} \le \mathcal{E} < (i+1)\Delta\mathcal{E}$. The total yield then becomes

$$Y_{\text{spec}} \approx \sum_i \int_{i\Delta\mathcal{E}}^{(i+1)\Delta\mathcal{E}} \psi(\mathcal{E})\, y_i\, d\mathcal{E}. \tag{6}$$

Since y_i is constant within the group, it can be taken outside the integral

$$Y_{\text{spec}} \approx \sum_i y_i \int_{i\Delta\mathcal{E}}^{(i+1)\Delta\mathcal{E}} \psi(\mathcal{E})\, d\mathcal{E}. \tag{7}$$

The integrals define the multigroup coefficients a_i

$$a_i = \int_{i\Delta\mathcal{E}}^{(i+1)\Delta\mathcal{E}} \psi(\mathcal{E})\, d\mathcal{E} \tag{8}$$

which correspond to the number of particles within the ith group, as illustrated in Fig. 5. Thus, Y_{spec} can be approximated as

$$Y_g = \sum_i a_i y_i. \tag{9}$$

Therefore, the multigroup formulation corresponds to a piecewise-constant approximation of the yield $y(\mathcal{E})$ and reduces the continuous spectral integral to a discrete weighted sum.

Acknowledgment

The authors acknowledge the National Laboratory for Scientific Computing (LNCC/MCTI, Brazil) for providing access to the Santos Dumont supercomputer (Project LPA-FARMA), which contributed to the research results reported in this article.

References

[1] W. Xu, J. Li, and L. Shi, "Study on producing radioisotopes based on fission or radiative capture method in a high flux reactor," *Nucl. Eng. Technol.*, vol. 56, no. 9, pp. 3585–3593, 2024.

[2] Y. Ge et al., "Measurement of Cumulative fission product yields on (235)U induced by 2.8 MeV neutrons," *Appl. Radiat. Isot.*, vol. 200, p. 110907, Oct. 2023, 10.1016/j.apradiso.2023.110907.

[3] M. Varga et al., "Role of single-photon emission computed tomography imaging in the diagnosis and treatment of chronic neck or back pain caused by spinal degeneration: A systematic review," *World Neurosurg.*, vol. 173, pp. 65–78, May 2023.

[4] V. S. Le, "^{99m}Tc generator development: Up-to-date ^{99m}Tc recovery technologies for increasing the effectiveness of ^{99}Mo utilisation," *Sci. Technol. Nucl. Ins.*, vol. 2014, p. 45252, Jan. 2014.

[5] E. Midgley. (2023). *Keeping the World's Ageing Research Reactors Running*. [Online]. Available: http://www.iaea.org/bulletin/keeping-the-worlds-ageing-research-reactors-running

[6] R. V. Noorden, "Radioisotopes: The medical testing crisis," *Nature*, vol. 504, no. 7479, pp. 202–204, Dec. 2013.

[7] B. S. Nunes, E. R. F. Rodrigues, J. A. P. Fruscalso, R. P. Nunes, A. Bonatto, and M. S. Alva-Sánchez, "Highly enriched uranium-free medical radioisotope production methods: An integrative review," *Appl. Sci.*, vol. 12, no. 24, p. 12569, 2022.

[8] T. M. Martin et al., "Production of ^{99}Mo/^{99m}Tc via photoneutron reaction using natural molybdenum and enriched 100Mo: Part 1, theoretical analysis," *J. Radioanal. Nucl. Ch.*, vol. 314, no. 2, pp. 1051–1062, 2017.

[9] F. Tárkányi et al., "Recommended nuclear data for medical radioisotope production: Diagnostic gamma emitters," *J. Radioanal. Nucl. Ch.*, vol. 319, no. 2, pp. 487–531, 2018.

[10] N. D. Vieira, E. P. Maldonado, A. Bonatto, R. P. Nunes, S. Banerjee, and F. A. Genezini, "Laser wakefield electron accelerator: Possible use for radioisotope production," in *Proc. SBFoton Int. Opt. Photon. Conf. (SBFoton IOPC)*, 2021, pp. 1–6, doi: 10.1109/SBFotonIOPC50774.2021.9461976.

[11] A. Shaikh, T. Dixit, A. Deshpande, and R. Krishnan, "GEANT4 based simulation study of converter and direct target design and optimization of target for ^{99}Mo production using 30 MeV electron linear accelerator," *Appl. Radiat. Isot.*, vol. 185, Jul. 2022, Art. no. 110239, doi: 10.1016/j.apradiso.2022.110239.

[12] M. Lin et al., "Optimization of target system for the production of ^{99}Mo via ^{100}Mo(γ,n)^{99}Mo reaction," *Appl. Radiat. Isot.*, vol. 202, Dec. 2023, Art. no. 111059, doi: 10.1016/j.apradiso.2023.111059.

[13] E. Esarey, C. B. Schroeder, and W. Leemans, "Physics of laser-driven plasma-based electron accelerators," *Rev. Mod. Phys.*, vol. 81, no. 3, pp. 1229–1285, 2009.

[14] T. Tajima and J. M. Dawson, "Laser electron accelerator," *Phys. Rev. Lett.*, vol. 43, no. 4, pp. 267–270, 1979.

[15] P.-W. Lai et al., "Laser wakefield acceleration of 10-MeV-scale electrons driven by 1-TW multi-cycle laser pulses in a sub-millimeter nitrogen gas cell," *Phys. Plasmas*, vol. 30, no. 1, 2023, Art. no. 010703.

[16] C. K. Birdsall and A. B. Langdon, *Plasma Physics via Computer Simulation*. New York, NY, USA: McGraw-Hill, 1985, p. 479.
[17] S. Agostinelli et al., "Geant4—A simulation toolkit," *Nucl. Instrum. Meth. A*, vol. 506, no. 3, pp. 250–303, 2003, doi: 10.1016/s0168-9002(03)01368-8.
[18] J. E. Allison et al., "Geant4 developments and applications," *IEEE T. Nucl. Sci.*, vol. 53, no. 1, pp. 270–278, Feb. 2006.
[19] E. Brochu, V. M. Cora, and N. de Freitas, "A tutorial on Bayesian optimization of expensive cost functions, with application to active user modeling and hierarchical reinforcement learning," 2010, *arXiv:1012.2599*.
[20] B. S. Nunes et al., "Bayesian optimization of laser wakefield acceleration in the self-modulated regime (SM-LWFA) aiming to produce molybdenum-99 via photonuclear reactions," *Phys. Plasmas*, vol. 32, no. 3, 2025, Art. no. 033101.
[21] B. S. Nunes, A. Bonatto, and R. E. Samad, "Decomposition method to speed up optimization loops containing Monte Carlo simulations to estimate radioisotope production," presented at the SBFoton Int. Opt. Photon. Conf. (SBFoton IOPC), 2024.
[22] R. Lehé, M. Kirchen, I. A. Andriyash, B. B. Godfrey, and J.-L. Vay, "A spectral, quasi-cylindrical and dispersion-free particle-in-cell algorithm," *Comput. Phys. Commun.*, vol. 203, pp. 66–82, Feb. 2016.
[23] E. P. Maldonado, R. E. Samad, A. Bonatto, R. P. Nunes, S. Banerjee, and N. D. Vieira, "Study of quasimonoenergetic electron bunch generation in self-modulated laser wakefield acceleration using TW or sub-TW ultrashort laser pulses," *AIP Adv.*, vol. 11, no. 6, 2021, Art. no. 065116.
[24] E. P. Maldonado, R. E. Samad, A. V. F. Zuffi, J. R. dos Santos, and N. D. Vieira, "Impact of He+N_2 concentration on self-modulated laser wakefield acceleration driven by pulses of a few TW," *J. Opt. Soc. Am. B*, vol. 40, no. 4, pp. C141–C147, 2023, doi: 10.1364/josab.482305.
[25] J. Perl, J. Shin, J. Schümann, B. Faddegon, and H. Paganetti, "TOPAS: An innovative proton Monte Carlo platform for research and clinical applications," *Med. Phys.*, vol. 39, no. 11, pp. 6818–6837, Nov. 2012.
[26] B. Faddegon et al., "The TOPAS tool for particle simulation, a Monte Carlo simulation tool for physics, biology and clinical research," *Phys. Medica*, vol. 72, pp. 114–121, Apr. 2020.
[27] J. E. Allison et al., "Recent developments in Geant4," *Nucl. Instrum. Meth. A*, vol. 835, pp. 186–225, Jul. 2016.
[28] J. J. Duderstadt and L. J. Hamilton, *Nuclear Reactor Analysis*. Hoboken, NJ, USA: Wiley, 1976, p. 563.
[29] A. Hébert, *Applied Reactor Physics*, 3rd ed., Montréal, QC, Canada: Les Presses de l'Université de Montréal, 2020.
[30] J. Lewins, *Importance, the Adjoint Function; The Physical Basis of the Variational and Perturbation Theory in Transport and Diffusion Problems*, 1st ed., New York, NY, USA: Pergamon, 1965.
[31] A. Mangiarotti and M. N. Martins, "A review of electron–nucleus bremsstrahlung cross sections between 1 and 10 MeV," *Rad. Phys. Chem.*, vol. 141, pp. 312–338, Jun. 2017.
[32] H. Bichsel and H. Schindler, "The interaction of radiation with matter," in *Particle Physics Reference Library: Volume 2: Detectors for Particles and Radiation*, vol. 2. Cham, Switzerland: Springer, 2020, pp. 5–44.

Coordenação de Aperfeiçoamento de Pessoal de Nível Superior (CAPES) - ROR identifier: 00x0ma614